

Tensorized orbitals for computational chemistry

Nicolas Jolly,¹ Yuriel Núñez Fernández,² and Xavier Waintal¹

¹*Univ. Grenoble Alpes, CEA, Grenoble INP, IRIG, PHELIQS, 38000 Grenoble, France*

²*Université Grenoble Alpes, CNRS, Institut Néel, 38000 Grenoble, France*

(Dated: October 7, 2024)

Choosing a basis set is the first step of a quantum chemistry calculation and it sets its maximum accuracy. This choice of orbitals is limited by strong technical constraints as one must be able to compute a large number of six dimensional Coulomb integrals from these orbitals. Here we use tensor network techniques to construct representations of orbitals that essentially lift these technical constraints. We show that a large class of orbitals can be put into “tensorized” form including the Gaussian orbitals, Slater orbitals, linear combination thereof as well as new orbitals beyond the above. Our method provides a path for building more accurate and more compact basis sets beyond what has been accessible with previous technology. As an illustration, we construct optimized tensorized orbitals and obtain a 85% reduction of the error on the energy of the H_2 molecules with respect to a reference double zeta calculation (cc-pvDz) of the same size.

The very first step of a first principles many-body calculation is to discretize the problem onto *some* finite basis set. On the quality of this discretization depends the maximum accuracy that may be reached in the calculation and therefore its usefulness for making predictions [1–3]. The commonly accepted target of $1.6mHa$ (around $500K$) for “chemical accuracy” typically requires large basis sets to approach the continuum sufficiently well. There exists an immense body of literature devoted to the construction of optimized basis sets for a wide variety of situations. Among others, those include plane waves, wavelets [4], Wannier function [5], Slater [6] and many flavours of Gaussian orbitals [1, 7–9]. Extrapolating the results to the Complete Basis Set (CBS) limit is still an important difficulty in practice [6, 10].

In the context of chemistry, the Gaussian orbitals overwhelmingly dominate the literature. Their popularity stems from two important properties. The first is (P1) their compactness, i.e. a few Gaussians centered on the different nuclei are sufficient to give a reasonably accurate approximation of the atomic orbitals. Second, and perhaps more importantly (P2), the 6-dimensional integrals appearing in the calculation of the electron-electron interaction matrix elements can be computed analytically for Gaussian orbitals. Property (P2) sounds somewhat technical. Yet, it is the crucial point that has allowed Gaussian orbitals to thrive and become ubiquitous in computational chemistry since these matrix elements are the starting points on which all further calculations are based. Despite these favourable aspects, Gaussian orbitals do have a number of important limitations: the convergence to the CBS limit is slow, core electrons are poorly described (in part because Gaussians lack the cusp that true atomic orbitals have close to the nuclei core; also the tail of the orbitals is in general not Gaussian) and so are delocalized orbitals above the ionization threshold.

In this letter, we do *not* propose another set of orbitals. Rather, we propose a novel *representation* of orbitals, using tensor networks [11–14]. This representation contains

a large class of orbitals that includes Gaussian orbitals, Slater orbitals, plane waves, new types calculated directly in real space as well as any combinations (e.g. molecular and natural orbitals). At the same time, it naturally solves the problem of computing the needed matrix elements (P2): once “tensorized”, the orbitals provide fast and robust access to all the usual mathematical objects needed by chemistry packages to proceed with the calculation.

Problem formulation. A molecule with N electrons is described by the positions \vec{R}_α and atomic number Z_α of its nuclei. We consider a basis set of M orbitals $\phi_i(\vec{r})$. Within this basis set, the many-body problem that one needs to solve has the following Hamiltonian,

$$H = \sum_{ij\sigma} H_{ij} c_{i\sigma}^\dagger c_{j\sigma} + \sum_{ijkl\sigma\sigma'} V_{ijkl} c_{i\sigma}^\dagger c_{j\sigma'}^\dagger c_{k\sigma'} c_{l\sigma} \quad (1)$$

where $c_{i\sigma}^\dagger$ ($c_{i\sigma}$) creates (destroys) an electron in orbital i and spin σ . They satisfy the anti-commutation rule $\{c_{i\sigma}^\dagger, c_{j\sigma}\} = \delta_{\sigma\sigma'} S_{ij}$ where S_{ij} is the overlap matrix. The problem is therefore defined by the objects S_{ij} , H_{ij} and V_{ijkl} whose expression in terms of the orbitals $\phi_i(\vec{r})$ is,

$$S_{ij} = \int d\vec{r} \phi_i(\vec{r}) \phi_j(\vec{r}) \quad (2)$$

$$H_{ij} = K_{ij} + P_{ij}$$

$$K_{ij} = \int d\vec{r} \phi_i(\vec{r}) \left[\frac{-\hbar^2}{2m} \Delta \right] \phi_j(\vec{r})$$

$$P_{ij} = - \int d\vec{r} \phi_i(\vec{r}) \left[\sum_\alpha \frac{Z_\alpha e^2}{4\pi\epsilon |\vec{r} - \vec{R}_\alpha|} \right] \phi_j(\vec{r}) \quad (3)$$

$$V_{ijkl} = e^2 \int d\vec{r}_1 d\vec{r}_2 \frac{\phi_i(\vec{r}_1) \phi_j(\vec{r}_2) \phi_k(\vec{r}_2) \phi_l(\vec{r}_1)}{4\pi\epsilon |\vec{r}_1 - \vec{r}_2|} \quad (4)$$

For a set of orbitals to be useful, one must be in position to compute Eqs. (2), (3) and (4) quickly and accurately. In particular the bottleneck of this calculation is given by the interaction matrix elements Eq. (4) which contains a large number $\propto M^4$ of 6-dimensional integrals.

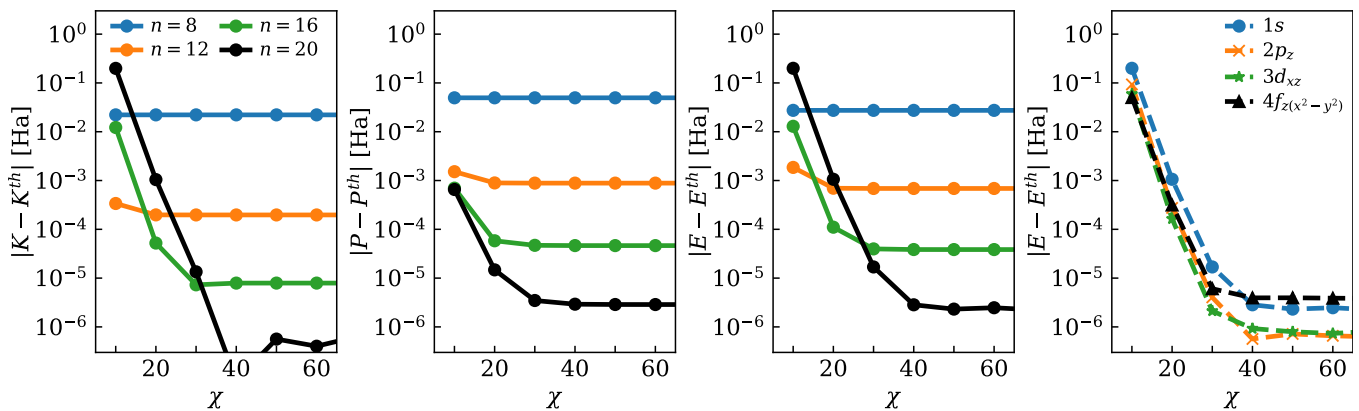


FIG. 1. Tensorisation of Slater orbitals. Error versus bond dimension χ for the energy of the exact $1s$ orbital of the hydrogen atom (first three panels) and other orbitals ($1s$, $2p_z$, $3d_{xz}$ and $4f_{z(x^2-y^2)}$, last panel). First three panels: error on the kinetic energy K , nuclei potential energy P and total energy $E = K + P$ for different grid discretization $n = 8, 12, 16$ and 20 . Last panel: $n = 20$ except for the $4f$ orbital for which $n = 22$. Energies in Hartree.

Quantics representation of an orbital. Let's consider an orbital $\phi(\vec{r})$ inside the cube $\vec{r} = (x, y, z) \in [0, b]^3$. The first step of the construction of the tensorized orbitals is to discretize the segment $[0, b]$ onto an *exponentially* dense grid of 2^n equally spaced points. Each of these points is labeled by n bits $x_1 x_2 \dots x_n \in \{0, 1\}^n$ such that

$$\frac{x}{b} = \frac{x_1}{2} + \frac{x_2}{2^2} + \dots + \frac{x_n}{2^n} \quad (5)$$

with similar equations for the y and z coordinates. One obtains a very large tensor $\Phi_{\vec{r}}$ with $3n$ indices indexing the $(2^n)^3$ different values of the orbital on the grid,

$$\Phi_{\vec{r}} \equiv \Phi_{x_1 x_2 \dots x_n y_1 y_2 \dots y_n z_1 z_2 \dots z_n} \quad (6)$$

Second, we represent the tensor $\Phi_{\vec{r}}$ as a tensor train (also known as matrix product state or MPS) in the so-called *grouped ordering* (other orderings are discussed in the supplementary materials),

$$\Phi_{\vec{r}} = \prod_{a=1}^n M_a(x_a) \prod_{a=1}^n M_{a+n}(y_a) \prod_{a=1}^n M_{a+2n}(z_a). \quad (7)$$

The tensor $\Phi_{\vec{r}}$ is now represented in terms of $3n$ matrices M_p of size (up to) $\chi \times \chi$. This is the quantics representation [15–17] of the orbital. Such a decomposition is always possible but the bond dimension χ may be exponentially large $\chi \sim 2^{3n/2}$. The magic of tensor trains is that for many mathematical objects the convergence of the tensor train with χ is very fast and very accurate results can be achieved with small values of χ ($\chi < 100$ in this work). In other words, many orbitals can be *compressed* using tensor trains. MPS plays a central role in computational many-body theory [11–13], in particular in the context of the density matrix renormalization algorithm (DMRG) [18]. The joined usage of MPS with the quantics representation is much more recent and has only recently started to be explored [19–24]. In the rest

of this letter, we propose three different algorithms to arrive at the tensorized representation of an orbital Eqs. (7). We will further discuss how, once the tensorized representation has been obtained, one can proceed with the calculation of S_{ij} , H_{ij} and V_{ijkl} thereby closing the gap to continue the calculation further with any many-body technique (e.g. Hartree-Fock, DMRG, coupled clusters...).

The Tensor Cross Interpolation (TCI) algorithm. The central algorithm that makes the present work possible is the recently introduced TCI learning algorithm [26, 27] that allows one to construct the tensor train from a few $\sim n\chi^2$ calls to the function $\phi(\vec{r})$. We rely on the *xfac* implementation and extensions of TCI described in detailed in [17, 28] to which we also refer for an introduction to the algorithm. For the needs of this letter, it is sufficient to know that the input of TCI is a tensor (in the form of a function that can be called for any values of the indices) and its output is the tensor train Eqs. (7) together with an estimate of the error (systematically controlled by increasing the bond dimension χ).

Slater orbitals. As a first illustration, we construct the tensorized representation of the exact Slater orbitals of the hydrogen atom using TCI. The $1s$ orbital is extremely simple, $\phi(\vec{r}) \propto \exp(-\sqrt{x^2 + y^2 + z^2}/a_0)$ (a_0 : bohr radius). Yet, computing precisely the different matrix elements for such orbitals centered around different nuclei positions is highly non-trivial [6, 29] which has restricted the use of Slater orbitals so far despite their potential benefits (correct cusps and tails). The first three panels of Fig. 1 show the error respectively for the kinetic energy K , potential energy P and total energy $E = K + P$ for the ground state of the hydrogen atom (the algorithms for these calculations will be detailed below). We observe that a very moderate value of χ is needed to achieve very precise accuracy $< 0.01m\text{Ha}$. On the other hand, the calculations of K and P requires a very fine

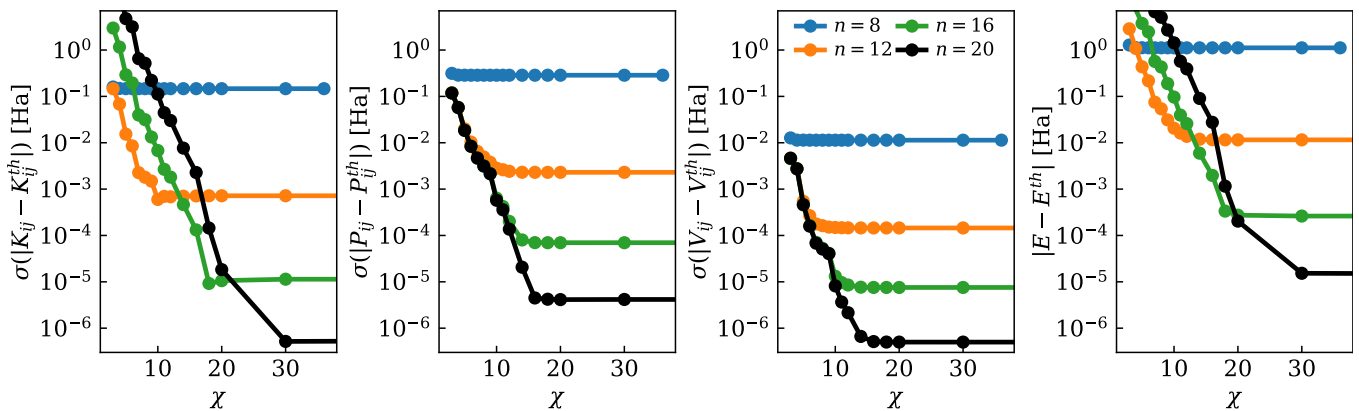


FIG. 2. Tensorisation of Gaussian orbitals: LiH molecule in the STO-6G basis set. Error versus bond dimension χ of the orbitals for the different matrix elements (first three panels, σ is the standard deviation) and overall CCSD(T) energy (last panel) for different discretization parameters $n = 8, 12, 16$ and 20 . Distance between the nuclei: $d_{Li-H} = 2.8571a_0$. Reference calculation: pyscf package [25].

grid with $n \geq 16$. This is not a issue with the quantics representation since the computational cost is linear in n . Indeed, the calculations with $n = 20$ (black curve) is only marginally more difficult than the calculation for $n = 12$ (orange) despite the fact that, formally, $n = 20$ corresponds to a grid that contains an astronomically large $\sim 10^{18}$ number of points ($\sim 10^{36}$ points for the 6-dimensional integrals). In the last panel of Fig. 1, we show the error for p , d and f orbitals. One finds that the accuracy depends only very weakly on the actual shape of the orbital. For the $4f$ orbital, we had to increase n up to $n = 22$ since this orbital is much more extended than $1s$. We found that TCI algorithm works equally well for all the orbitals that we have tested; they only need to be known explicitly, i.e. one can compute $\phi(\vec{r})$ for any value of \vec{r} . This includes in particular any combination of Gaussians as we have checked explicitly.

Algorithms for the computation of S_{ij} , H_{ij} and V_{ijkl} . The crucial property of tensorized orbitals is the ability to compute the interaction matrix elements needed for subsequent many-body calculations at an exponentially reduced $O(n)$ cost. The simplest one is S_{ij} . Indeed, in the framework of MPS, $S_{ij} = V_0 \sum_{\vec{r}} \Phi_{\vec{r}}^i \Phi_{\vec{r}}^j$ is simply the scalar product between two MPS. Here $V_0 \equiv b^3/2^{3n}$ is the elementary grid cell volume. The algorithm for contracting this tensor network belongs to the standard toolbox of MPS [11] and has a mild complexity $\sim n\chi^3$.

Second is the kinetic energy K_{ij} . We discretize the Laplacian on the grid using finite difference, i.e. $\partial^2 \phi / \partial x^2 \approx [\phi(x + 1/2^n) - 2\phi(x) + \phi(x - 1/2^n)] / 2^{2n}$. In the quantics representation, this second derivative can be written explicitly as a ‘‘Matrix Product Operator’’ (MPO, an MPO is to matrices what MPS are to vectors) $\Delta_{\vec{r}_1 \vec{r}_2}$ with a very small bond dimension $\chi = 4$ [22]. The calculation of K_{ij} is therefore put in the form $K_{ij} = V_0 \sum_{\vec{r}_1 \vec{r}_2} \Phi_{\vec{r}_1}^i \Delta_{\vec{r}_1 \vec{r}_2} \Phi_{\vec{r}_2}^j$ which is a MPS.MPO.MPS

product. We are back to the standard algorithms of the MPO/MPS toolbox.

Next comes the contribution from the nuclei potential P_{ij} . The functions $1/|\vec{r} - \vec{R}_\alpha|$ are given to the TCI algorithm which produces an MPS $P_{\vec{r}}^\alpha$. Our numerical experiments show a fast convergence: the relative accuracy for $P_{\vec{r}}^\alpha$ is around 10^{-3} for $\chi = 60$ and 10^{-5} for $\chi = 100$. We arrive at $P_{ij} = V_0 \sum_{\vec{r}, \alpha} \Phi_{\vec{r}}^i P_{\vec{r}}^\alpha \Phi_{\vec{r}}^j$ which is a direct extension of the MPS.MPS scalar product. It proves more efficient to compute this matrix element for every nucleus α and then sum the whole, because having one single MPS for all the potentials tends to require bigger χ for a given accuracy.

Last, we need to calculate the interaction matrix elements V_{ijkl} . The function $1/|\vec{r}_1 - \vec{r}_2|$ is given to the TCI algorithm which produces an MPO $U_{\vec{r}_1, \vec{r}_2}$. Here as well, $\chi \approx 100$ is needed to reach a relative accuracy of 10^{-4} . We arrive at $V_{ijkl} = V_0^2 \sum_{\vec{r}_1 \vec{r}_2} \Phi_{\vec{r}_1}^i \Phi_{\vec{r}_1}^j U_{\vec{r}_1 \vec{r}_2} \Phi_{\vec{r}_2}^k \Phi_{\vec{r}_2}^l$. To evaluate these matrix elements we first form the element-wise product $\Phi_{\vec{r}}^i \Phi_{\vec{r}}^j$ for all pairs ij , then compress them using SVD into an MPS $\Phi_{\vec{r}}^{ij}$. Then, we’re back to the calculations of MPS.MPO.MPS products $V_{ijkl} = V_0^2 \sum_{\vec{r}_1 \vec{r}_2} \Phi_{\vec{r}_1}^{ij} U_{\vec{r}_1 \vec{r}_2} \Phi_{\vec{r}_2}^{kl}$. This completes the suite of algorithms.

Validation of the whole algorithmic chain. To validate the entire procedure, we make use of Gaussian orbitals for which all these contributions are known analytically. We use the package pyscf [25] for this benchmark. Figure 2 shows a calculation of all the matrix elements for the LiH molecule in the STO-6G basis set (first three panels) together with the resulting CCSD(T) calculation (last panel). This is a mere validation that we can calculate the *inputs* of the many-body problem, to be solved by any suitable mean. We find that $n = 16$ and $\chi = 17$ (with $\chi \approx 60$ for the MPS $P_{\vec{r}}^\alpha$ and MPO $U_{\vec{r}_1, \vec{r}_2}$) are sufficient to reach chemical accuracy for all matrix elements as well

as the final total energy. Interestingly though, a slightly coarser discretization of $(2^{12})^3 \approx 6 \cdot 10^{10}$ points is not sufficient, showing that the arbitrary resolution available with tensorized orbitals is really needed.

For a target accuracy at 1mHa on the energies ($n = 16$, $\chi = 17$), the computing time to compute all matrix elements is $\text{CPU} \approx n[78A(M) + 0.18B(M)]$ milli-seconds on a single computing core with $A(M) = M(M+1)/2$ and $B(M) = M(M+1)(M^2 + M + 1)/8$ counting the number of different elements in respectively S_{ij} and V_{ijkl} . This translates into about 30s for the present example which can be trivially parallelized and further optimized (see supp. mat.). While this is not competitive with the specific method for Gaussian orbitals, it is fast enough for *not* being the bottleneck of the calculation, in particular when an accurate many-body solver such as CCSD(T) [CPU $\sim M^7$ at half filling] is used.

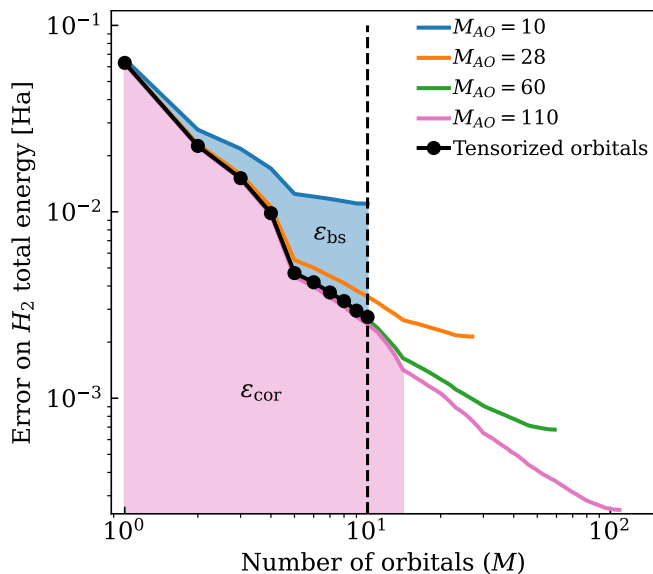


FIG. 3. Error on the ground energy of the H_2 molecule for different basis sets. The calculation uses M orbitals constructed optimally out of M_{AO} atomic orbitals (colored lines) or using our enrichment algorithm (black circles, $n = 20$). Pink shaded area: ϵ_{cor} ; Blue shaded area: ϵ_{bs} . The interatomic distance is $d_{H-H} = 1.4013 a_0$, the reference energy is $E_0 = -1.17447498$ Ha [30] and the many-body problem is treated exactly with `pyscf`.

Basis set versus correlation errors. Calculations performed with five zeta gaussian basis sets (e.g. cc-pv5z) can be considered as accurate while double zeta basis sets (e.g. cc-pvDz) suffer from strong inaccuracies [31]. The problem is that even for a moderately big molecule like benzene, it is difficult to go beyond double zeta while properly accounting for correlations [32]. The question is therefore simple: can tensorised orbitals provide some of the five zeta accuracy while working with basis sets of the size of the double zeta? More precisely, one may work in a regime where M_{AO} (the number of underlying atomic

orbitals, say Gaussians and/or Slater) is much larger than the number of (molecular or natural) orbitals M used in the many-body solver (the bottleneck of the calculation). We define the error $\epsilon(M, M_{AO}) = |E(M, M_{AO}) - E(M = \infty, M_{AO} = \infty)| = \epsilon_{\text{bs}} + \epsilon_{\text{cor}}$ as the sum of the "basis set" error $\epsilon_{\text{bs}}(M, M_{AO}) = |E(M, M_{AO}) - E(M, M_{AO} = \infty)|$ and the "correlation" error $\epsilon_{\text{cor}}(M) = |E(M, M_{AO} = \infty) - E(M = \infty, M_{AO} = \infty)|$. Typical quantum chemistry calculations use $M_{OA} \sim M$. However a tensorized orbital can be constructed out of tens or hundreds of atomic orbital, it is still a unique orbital and performing calculations with it is essentially independent on how it has been constructed; hence, one may potentially get rid of the ϵ_{bs} error.

Let us estimate ϵ_{bs} and ϵ_{cor} for the H_2 molecule. We perform the following calculation: (i) We perform a CCSD calculation (exact here since there are only 2 electrons) of H_2 in the cc-pvXz basis, X=D,T,Q,5 corresponding to $M_{AO} = 10, 28, 60$ and 110. (ii) For each calculation, we diagonalize the one-body density matrix $\rho_{ij} = \langle c_i^\dagger c_j \rangle$. Its eigenstates are the natural orbitals of the problem [33] and the eigenvalues the corresponding filling factors. (iii) We perform a second series of CCSD calculation keeping only M natural orbitals with the highest filling factor. The results are shown in Fig. 3 (thin lines). As one increases the ratio $M_{AO}/M \rightarrow \infty$, one observes the convergence towards a universal curve where the error is entirely controlled by the dynamical correlations – not by the choice or size of the basis set – this is the continuum limit where $\epsilon = \epsilon_{\text{cor}}$. Note that this continuum limit is *not* the usual CBS limit, since the latter also implies taking $M \rightarrow \infty$. For $M = 10$ the correlation error is of $\epsilon_{\text{cor}} = 2.5$ mHa, it is more than four times smaller than the full error $\epsilon = 11.1$ mHa of the cc-pvDz calculation that uses $M = M_{AO} = 10$ (end of the blue line). So far, this calculation is contrived because we performed an expensive CCSD calculation with $M = 110$ in step (i). Nevertheless it indicates that the potential for a large gain in accuracy is present, we just need an algorithm to build the optimized orbitals directly. We have repeated the procedure (i)-(iii) for several molecules (see Supp. Mat.) and consistently found a large value of ϵ_{bs} of more than 100mHa for the cc-pvDz basis. More importantly, the remaining error $\epsilon_{\text{corr}}(M)$ depends only on M (not on the precise and delicate construction of the basis set) and is therefore free of any arbitrariness in its construction. Altogether we consistently found that the final error with respect to CBS could be lowered by a factor ten or more (see Supp. Mat.) at no additional computational cost.

The preferred way to optimize the orbitals will probably be directly in real space (see below) independently from Gaussians. However, as a first attempt, we show here an enrichment algorithm that provides the optimum error for $M = 10$ without paying the high price of step (i) (black circles in Fig. 3). The enrichment algorithm goes as follows: (a) We choose the $M^* = 15$ atomic or-

Error on the ground state energy				
Method	H		H_2^+ ($d_{H-H} = 2 a_0$)	HeH^{2+} ($d_{He-H} = 1.4634 a_0$)
cc-pvDz basis set	+0.72 mHa	[28 gaussians]	+ 2.37 mHa [56 gaussians]	+ 7.17 mHa [56 gaussians]
cc-pv5z basis set	+5.46 μ Ha	[110 gaussians]	+14.5 μ Ha [220 gaussians]	+64.6 μ Ha [220 gaussians]
DMRG with $n = 20$	+1.45 μ Ha	$[\chi = 54]$	+1.22 μ Ha $[\chi = 53]$	$\equiv 0 \mu$ Ha $[\chi = 58]$
Reference energy	- 0.5 Ha		- 1.1026342144949 Ha [30]	- 2.7136469(2) Ha

TABLE I. Single orbital calculation: linear combination of Gaussians versus DMRG. Error on ground state energies of a single electron in different ions. The cc-pvDz and cc-pv5z rows are obtained with `pyscf` simulations. The MPS are calculated with the DMRG algorithm. A $n = 20$ -MPS performs better than the most elaborate Gaussian basis set (cc-pv5z) by an order of magnitude. For HeH^{2+} , the energy obtained by DMRG was more precise than what we could find in the literature, we use it as reference.

bitals of lowest energy and remove them from the cc-pvQz basis set. (b) We solve the many-body problem with these orbitals. (c) We construct the corresponding natural orbitals. (d) We keep the $M < M^*$ natural orbital of highest filling factor; we enrich the basis set with $M^* - M$ new atomic orbitals taken from the remaining ones of the cc-pvQz basis set. (e) We repeat steps (b,c,d) until there are no orbitals left in the cc-pvQz basis set. While this algorithm is rather crude, we find that it provides the optimum error for $M = 10$ while *never* solving the many-body problem for more than $M^* \sim M$ orbitals. This is a first step towards getting rid entirely of the basis set error.

Constructing tensorized orbitals directly from real space calculations. Ultimately, we would like to construct the optimized tensorized orbitals directly following e.g. algorithms in the spirit of [34]. We end this letter by taking a first step in this direction, calculating the (tensorized) ground state of the H_2^+ and HeH^{2+} ions (one electron and two nuclei) directly using MPO/MPS techniques. This is an interesting case because chemical bonds are not easy to represent with high accuracy with Gaussian orbitals (see suppl. mat.). We seek a tensorized orbital $\Phi_{\vec{r}}$ that minimizes the energy of the H_2^+/HeH^{2+} ion. Here, we take advantage of the fact that the Schrödinger equation for the wavefunction of the electron has already been put into MPO/MPS form, i.e. we are looking for the lowest eigenenergy of the one electron Hamiltonian, or equivalently the minimum of,

$$E = V_0 \min_{\Phi_{\vec{r}}} \sum_{\vec{r}_1, \vec{r}_2} \Phi_{\vec{r}_1} [\Delta_{\vec{r}_1, \vec{r}_2} + P_{\vec{r}_1} \delta_{\vec{r}_1, \vec{r}_2}] \Phi_{\vec{r}_2} \quad (8)$$

where $\delta_{\vec{r}_1, \vec{r}_2}$ is the kronecker symbol. Performing such a minimization is exactly what the celebrated DMRG algorithm does, although usually in a totally different context (each index usually corresponds to the occupation of an orbital while here they label the different scales of a one-particle problem). Hence we can rely on any existing implementation of DMRG to calculate the orbital (here the quimb package [35]). The results are shown in Table I. DMRG easily outperforms the precision that we could

obtain with two hundred Gaussians [8] by one order of magnitude. More importantly, the result is a single orbital whose rank is not significantly higher than those of simple Gaussians or Slaters.

Conclusions. Tensor network techniques were invented in the context of solving many-body problems, mostly in one dimension, and for a long time were mostly confined to this application. In the last few years important technical developments have appeared and these techniques are stepping out of their original context. In particular the TCI algorithm provides a natural bridge to map problems apparently unrelated to tensor networks onto the MPO/MPS toolbox. In this article we have shown that a combination of the quantics representation, TCI and the traditional MPO/MPS toolbox provides all the necessary ingredients to represent atomic, molecular or natural orbitals with very high - perhaps unprecedented - accuracy. This methodology provides new possibilities for constructing accurate basis sets, lifting the strong constraint of having to express them solely in terms of Gaussians. Future work will include the integration of these tensorized orbitals, ideally within a standardized format, with the existing quantum chemistry packages as well as the exploration of new ways to construct basis sets opened by this format.

Acknowledgment. We thank Miles Stoudenmire, Emanuel Gull and Steve White for interesting discussions. XW acknowledges funding from the Plan France 2030 ANR-22-PETQ-0007 ‘‘EPIQ’’, from the French ANR DADDI, from the AI program of the French MESRI and from the CEA-FJZ AIDAS program.

-
- [1] D. E. Woon and J. Dunning, Thom H., Gaussian basis sets for use in correlated molecular calculations. V. Core-valence basis sets for boron through neon, *The Journal of Chemical Physics* **103**, 4572 (1995), https://pubs.aip.org/aip/jcp/article-pdf/103/11/4572/10777979/4572_1_online.pdf.
- [2] K. A. Peterson, D. Feller, and D. A. Dixon, Chemical accuracy in ab initio thermochemistry and spec-

- troscopy: current strategies and future challenges, *Theoretical Chemistry Accounts* **131**, 1079 (2012).
- [3] Cancès, Eric and Dusson, Geneviève, Discretization error cancellation in electronic structure calculation: toward a quantitative study, *ESAIM: M2AN* **51**, 1617 (2017).
- [4] S. R. White, Hybrid grid/basis set discretizations of the schrödinger equation, *The Journal of Chemical Physics* **147**, 10.1063/1.5007066 (2017).
- [5] G. Pizzi, V. Vitale, R. Arita, S. Blügel, F. Freimuth, G. Géranton, M. Gibertini, D. Gresch, C. Johnson, T. Koretsune, J. Ibañez-Azpiroz, H. Lee, J.-M. Lihm, D. Marchand, A. Marrazzo, Y. Mokrousov, J. I. Mustafa, Y. Nohara, Y. Nomura, L. Paulatto, S. Poncé, T. Ponweiser, J. Qiao, F. Thöle, S. S. Tsirkin, M. Wierzbowska, N. Marzari, D. Vanderbilt, I. Souza, A. A. Mostofi, and J. R. Yates, Wannier90 as a community code: new features and applications, *Journal of Physics: Condensed Matter* **32**, 165902 (2020).
- [6] A. Förster and L. Visscher, Gw100: A slater-type orbital perspective, *Journal of Chemical Theory and Computation* **17**, 5080 (2021), pMID: 34236172, <https://doi.org/10.1021/acs.jctc.1c00308>.
- [7] W. J. Hehre, R. F. Stewart, and J. A. Pople, Self-Consistent Molecular-Orbital Methods. I. Use of Gaussian Expansions of Slater-Type Atomic Orbitals, *The Journal of Chemical Physics* **51**, 2657 (2003).
- [8] F. Jensen, Atomic orbital basis sets, *Wiley Interdisciplinary Reviews: Computational Molecular Science* **3** (2013).
- [9] Y. Zhou, E. Gull, and D. Zgid, Material-specific optimization of gaussian basis sets against plane wave data, *Journal of Chemical Theory and Computation* **17**, 5611 (2021), pMID: 34448587, <https://doi.org/10.1021/acs.jctc.1c00491>.
- [10] F. Bruneval, N. Dattani, and M. J. van Setten, The gw miracle in many-body perturbation theory for the ionization potential of molecules, *Frontiers in Chemistry* **9**, 10.3389/fchem.2021.749779 (2021).
- [11] U. Schollwöck, The density-matrix renormalization group in the age of matrix product states, *Ann. Phys.* **326**, 96 (2011).
- [12] R. Orús, A practical introduction to tensor networks: Matrix product states and projected entangled pair states, *Annals of Physics* **349**, 117 (2014).
- [13] R. Orús, Tensor networks for complex quantum systems, *Nature Reviews Physics* **1**, 538 (2019).
- [14] J. C. Bridgeman and C. T. Chubb, Hand-waving and interpretive dance: an introductory course on tensor networks, *Journal of Physics A: Mathematical and Theoretical* **50**, 223001 (2017).
- [15] I. V. Oseledets, Approximation of matrices with logarithmic number of parameters, *Doklady Mathematics* **80**, 653 (2009).
- [16] B. N. Khoromskij, $\mathcal{O}(d \log n)$ -quantics approximation of $n - d$ tensors in high-dimensional numerical modeling, *Constructive Approximation* **33**, 257 (2011).
- [17] Y. N. Fernández, M. K. Ritter, M. Jeannin, J.-W. Li, T. Kloss, T. Louvet, S. Terasaki, O. Parcollet, J. von Delft, H. Shinaoka, and X. Waintal, Learning tensor networks with tensor cross interpolation: new algorithms and libraries (2024), arXiv:2407.02454 [physics.comp-ph].
- [18] S. R. White, Density matrix formulation for quantum renormalization groups, *Phys. Rev. Lett.* **69**, 2863 (1992).
- [19] M. Lubasch, P. Moinier, and D. Jaksch, Multigrid renormalization, *Journal of Computational Physics* **372**, 587 (2018).
- [20] J. J. García-Ripoll, Quantum-inspired algorithms for multivariate analysis: from interpolation to partial differential equations, *Quantum* **5**, 431 (2021).
- [21] E. Ye and N. F. G. Loureiro, Quantum-inspired method for solving the vlasov-poisson equations, *Phys. Rev. E* **106**, 035208 (2022).
- [22] N. Gourianov, M. Lubasch, S. Dolgov, Q. Y. van den Berg, H. Babaei, P. Givi, M. Kiffner, and D. Jaksch, A quantum inspired approach to exploit turbulence structures, *Nature Computational Science* **2**, 30 (2022).
- [23] H. Shinaoka, M. Wallerberger, Y. Murakami, K. Nogaki, R. Sakurai, P. Werner, and A. Kauch, Multi-scale space-time ansatz for correlation functions of quantum systems, arXiv:2210.12984 [cond-mat.str-el] (2022).
- [24] M. K. Ritter, Y. N. Fernández, M. Wallerberger, J. von Delft, H. Shinaoka, and X. Waintal, Quantics tensor cross interpolation for high-resolution, parsimonious representations of multivariate functions in physics and beyond (2023), arXiv:2303.11819 [physics.comp-ph].
- [25] Q. Sun, T. C. Berkelbach, N. S. Blunt, G. H. Booth, S. Guo, Z. Li, J. Liu, J. D. McClain, E. R. Sayfutyarova, S. Sharma, S. Wouters, and G. K.-L. Chan, Pyscf: the python-based simulations of chemistry framework, *WIREs Computational Molecular Science* **8**, e1340 (2018), <https://doi.org/10.1002/wcms.1340>.
- [26] I. V. Oseledets, Tensor-train decomposition, *SIAM Journal on Scientific Computing* **33**, 2295 (2011).
- [27] S. Dolgov and D. Savostyanov, Parallel cross interpolation for high-precision calculation of high-dimensional integrals, *Computer Physics Communications* **246**, 106869 (2020).
- [28] Y. Núñez Fernández, M. Jeannin, P. T. Dumitrescu, T. Kloss, J. Kaye, O. Parcollet, and X. Waintal, Learning Feynman diagrams with tensor trains, *Phys. Rev. X* **12**, 041018 (2022).
- [29] G. te Velde, F. M. Bickelhaupt, E. J. Baerends, C. Fonseca Guerra, S. J. A. van Gisbergen, J. G. Snijders, and T. Ziegler, Chemistry with adf, *Journal of Computational Chemistry* **22**, 931 (2001), <https://onlinelibrary.wiley.com/doi/pdf/10.1002/jcc.1056>.
- [30] W. Kolos and L. Wolniewicz, Improved Theoretical Ground-State Energy of the Hydrogen Molecule, *The Journal of Chemical Physics* **49**, 404 (1968), <https://pubs.aip.org/aip/jcp/article-pdf/49/1/404/18856813/404.1-online.pdf>.
- [31] W. Ren, W. Fu, X. Wu, and J. Chen, Towards the ground state of molecules via diffusion monte carlo on neural networks, *Nature Communications* **14**, 10.1038/s41467-023-37609-3 (2023).
- [32] J. J. Eriksen, T. A. Anderson, J. E. Deustua, K. Ghanem, D. Hait, M. R. Hoffmann, S. Lee, D. S. Levine, I. Magoulas, J. Shen, N. M. Tubman, K. B. Whaley, E. Xu, Y. Yao, N. Zhang, A. Alavi, G. K.-L. Chan, M. Head-Gordon, W. Liu, P. Piecuch, S. Sharma, S. L. Ten-no, C. J. Umrigar, and J. Gauss, The ground state electronic energy of benzene, *The Journal of Physical Chemistry Letters* **11**, 8922 (2020), pMID: 33022176, <https://doi.org/10.1021/acs.jpcllett.0c02621>.
- [33] E. R. Davidson, Properties and uses of natural orbitals, *Rev. Mod. Phys.* **44**, 451 (1972).
- [34] E. F. Valeev, R. J. Harrison, A. A. Holmes, C. C. Peterson, and D. A. Penchoff, Direct determination

of optimal real-space orbitals for correlated electronic structure of molecules, *Journal of Chemical Theory and Computation* **19**, 7230 (2023), pMID: 37791808, <https://doi.org/10.1021/acs.jctc.3c00732>.

- [35] J. Gray, quimb: a python library for quantum information and many-body calculations, *Journal of Open Source Software* **3**, 819 (2018).
- [36] T. Ayral, T. Louvet, Y. Zhou, C. Lambert, E. M. Stoudenmire, and X. Waintal, Density-matrix renormalization group algorithm for simulating quantum circuits with a finite fidelity, *PRX Quantum* **4**, 020304 (2023).
- [37] V. M. F. Verstraete and J. Cirac, Matrix product states, projected entangled pair states, and variational renormalization group methods for quantum spin systems, *Advances in Physics* **57**, 143 (2008), <https://doi.org/10.1080/14789940801912366>.
- [38] F. Weigend, A fully direct ri-hf algorithm: Implementation, optimised auxiliary basis sets, demonstration of accuracy and efficiency, *Phys. Chem. Chem. Phys.* **4**, 4285 (2002).

Supplementary material

Some pointers to the relevant MPO/MPS literature.

This article makes heavy use of several tensor network concepts that are well known in some communities but new in others. Here, we gather a few pointers to the literature that may be useful for people new to the field.

- A concise and gentle introduction to tensor networks, in the context of quantum computing, may be found in the Appendix A of [36].
- An introduction to the quantics representation of functions as tensors can be found in [17].
- an introduction to the Tensor Cross Interpolation algorithm can be found in Section 3 of [28]. Another introduction, together with an advanced presentation of the most advanced algorithms can be found in [17].
- Most of the literature on MPO/MPS algorithms focus on many-body solvers for one dimensional models of interacting spins or electrons. Classic reviews include [11, 14, 37]. The algorithms presented in these references, such as DMRG, TEBD or TDVP can be directly used in the quantics representation although it might be interesting to build special versions optimized for quantics.
- Interesting material can also be found in the documentation of tensor network open source libraries such as iTensor, TenPy (<https://tenpy.readthedocs.io/en/latest/>) and tensor4all [17]

Controlling the accuracy of TCI-built MPS.

During the TCI construction of a tensorized orbital $\phi_{\text{MPS}}(\vec{r})$ from a known orbital $\phi(\vec{r})$ (e.g. a Slater or a sum of Gaussians), we monitor three different types of error:

- The *in-sample* error ϵ_{is} corresponds to the maximum error observed during the TCI construction between the actual function that is being tensorized and its tensorized approximation. We define it as,

$$\epsilon_{is} = \max_{\vec{r}_i \in Q} |\phi(\vec{r}_i) - \phi_{\text{MPS}}(\vec{r}_i)| \quad (9)$$

where Q is the set of observed points used by TCI in the interpolation process. In machine learning terminology, this would be called a training set error albeit a very conservative one since the algorithm consistently seeks points where this error is maximum.

- The *out-of-sample* error ϵ_{os} corresponds to the average error on a set P of N_P randomly selected points ($N_P = 500$ typically). In order to select these points in relevant regions (where e.g. the function is non vanishing), we obtain them by sampling $|\phi(\vec{r})|^2$ using the Metropolis-Hastings algorithm. We define this error as :

$$\epsilon_{os} = \frac{1}{N_P} \sum_{\vec{r}_i \in P} |\phi(\vec{r}_i) - \phi_{\text{MPS}}(\vec{r}_i)| \quad (10)$$

In machine learning terminology, this error would correspond to the error associated with the test set.

- The *normalization error* ϵ_{norm} (or more generally integral errors) is a global measure of the error. It is defined, for an orbital that is supposed to be normalized to unity, as

$$\epsilon_{norm} = \left| V_0 \sum_{\vec{r}} |\phi_{\text{MPS}}(\vec{r})|^2 - 1 \right| \quad (11)$$

We have similar definitions for other objects such as the Coulomb potential $1/|\vec{r}_1 - \vec{r}_2|$ or other objects that need to be cast onto MPO/MPS. We observe that all these errors decrease exponentially with the rank χ . In the case of the normalization error, the error eventually saturates to $\epsilon_{norm} \sim 1/2^n$ when it becomes limited by the discretization.

Fig. 4 shows these three errors for the case of the 1s orbital of the hydrogen atom for $n = 12, 16$ and 20 . All three error closely follow each other within a $O(1)$ multiplicative factor and display a very fast decay. For a given χ , the error is typically smaller by running TCI for a larger value, say $\chi' = 150 > \chi$ then compressing the result down to χ using SVD. This is the preferred

algorithm when the time to obtain the MPS is not the limiting step. Both this algorithm (full lines) and the direct approach with rank χ are shown in Fig. 4c

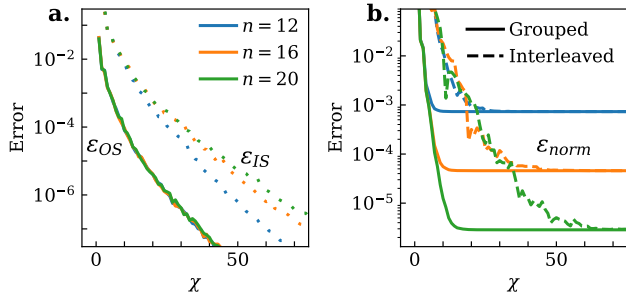


FIG. 4. Errors of the MPS interpolating the 1s orbital of the Hydrogen atom versus its rank χ . **a.** In sample error (ϵ_{IS}) in dotted lines and out of sample error (ϵ_{OS}) in solid lines. Both are converging exponentially to 0. **b.** Error on the integral. Here, the exact integral is $\int \phi(x)\phi^\dagger(x)dx = 1$. **c.** ϵ_{norm} obtained by running TCI with a high rank 150 then compressing the MPS down to χ (full lines, default algorithm) compared to running directly TCI with rank χ (dashed lines).

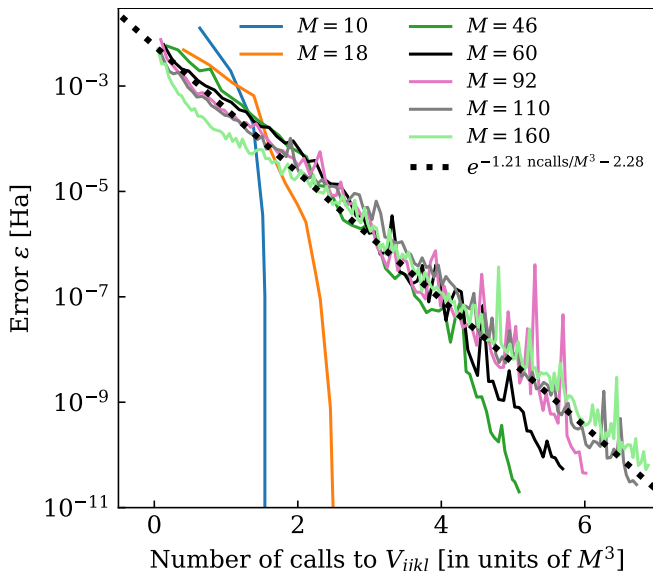


FIG. 5. Error of the MPS interpolating the V_{ijkl} tensor during its construction with the TCI algorithm. As the number of calls to the tensor grows, the error drops exponentially. The interpolation of the data is shown with the dotted line. The slope of the line is -1.21 . The error is taken on samples of 10^4 points taken randomly in the tensor.

Direct compression of the V_{ijkl} tensor using TCI.

Large chemistry computations often require thousands of orbitals. For such large values of M , storing the V_{ijkl}

tensor in memory can become a bottleneck, as it contains $\sim M^4$ elements. The computing part can also become a significant part of the computation, even when using Gaussians, in particular for relatively light methods such as DFT. A common approach to alleviate this problem is to build a so-called "auxiliary basis" made of $O(M)$ Gaussians [38]. The products $\phi_{ij}(\vec{r}) \equiv \phi_i(\vec{r})\phi_j(\vec{r})$ are expanded onto this auxiliary basis set (the associated tensor has $\sim M^3$ elements). Then, only the Coulomb matrix elements between the auxiliary orbitals need to be computed. This approach reduces the memory footprint to $\sim M^3$ and works well but it requires the fine tuning of the auxiliary basis which is a source of extra loss in accuracy.

Here, we use a different approach and compress V_{ijkl} directly using TCI, therefore never building the full tensor. Note that this approach takes advantage of a unique feature of TCI with respect to other compressing approaches such as those based on the singular value decomposition: the algorithm does not need the entire tensor V_{ijkl} to compress it, it only need to be able to compute some of its elements.

Fig. 5 shows our numerical experiment for a few test molecules. We found that for a targetted error ϵ (Frobenius norm), the number of V_{ijkl} elements that need to be computed scales as $\sim (-\log \epsilon)M^3$, i.e. offers the same compression scaling as the auxiliary basis set approach. It has two distinct advantages however: its accuracy can be easily controlled and the method is fully automatic and agnostic with respect to the underlying basis set (or lack of). This approach can be used to reduce the leading $O(M^4)$ contribution to the calculation of the Coulomb matrix elements.

Matrix elements of the LiH Molecule

In the main text, we show the convergence of the matrix elements and the total energy (at the CCSD(T) level) for the LiH molecule in the STO-6g basis set. The input of the many-body calculation are the integrals S_{ij}^{MPS} , K_{ij}^{MPS} , P_{ij}^{MPS} , V_{ijkl}^{MPS} that need to be computed for the tensorized orbitals. Fig. 6 displays these matrices for the $n = 20$ case (upper panels) along with the corresponding error on each matrix element (lower panels). This is the same data as Fig. 2. We consistently find that that the error is more than 5 orders of magnitudes smaller than the value of the integrals.

Accuracy of the matrix elements versus tolerance.

In the main text, we showcased the errors of the matrix elements versus rank χ . In practical calculations, we do not fix χ but rather a tolerance τ for the observed error requiring $\epsilon < \tau$ in all steps of the calculation. Indeed,

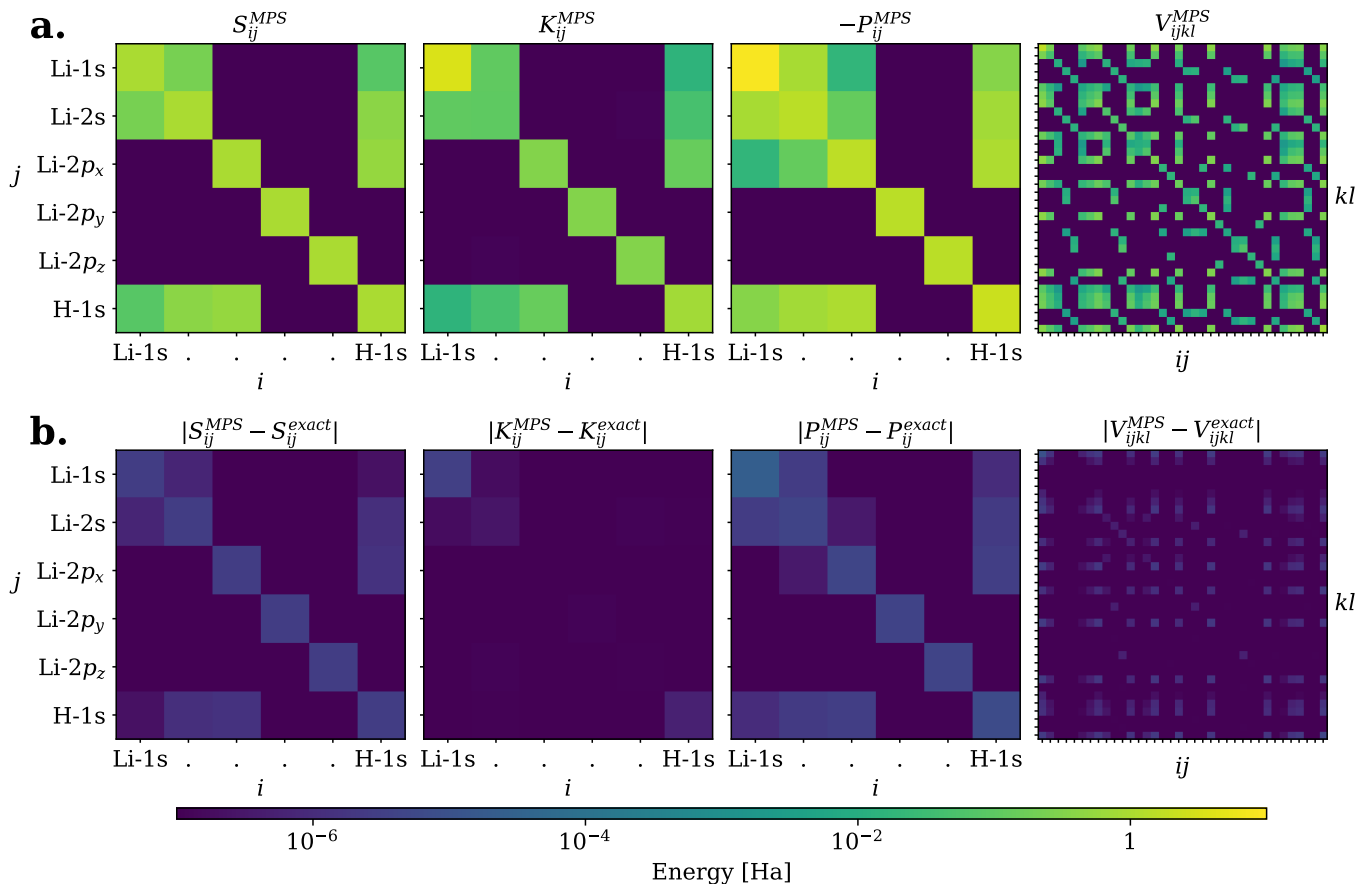


FIG. 6. Upper panels **a.**: Different matrix elements for the LiH molecule in the STO-6g basis set. Lower panels **b.**: corresponding error. This is the same data as for Fig. 2 of the main text in the $n = 20$ case. From left to right: S_{ij} , K_{ij} , P_{ij} and V_{ijkl} .

different MPS can have different ranks for the same targeted tolerance, so this approach is much more robust. Fig. 7 shows the error of the different matrix elements versus τ for the H_2 molecule within the cc-pvDz basis. We observe that, here, having $n = 12$ and $\tau = 10^{-3}$ is actually enough to obtain 1mHa accuracy on the matrix elements and eventually on the final energy.

Natural Orbitals.

In Fig. 3, we have used natural orbitals to construct an optimum basis set of M orbitals out of a much larger set of M_{AO} (Gaussian) atomic orbitals. Introducing the one-body density matrix $\rho_{ij} \equiv \langle c_i^\dagger c_j \rangle$, the natural orbitals $\phi_\alpha^N(\vec{r})$ are obtained by diagonalizing ρ ,

$$\rho_{ij} = \sum_{\alpha} U_{\alpha i}^* \lambda_{\alpha} U_{\alpha j} \quad (12)$$

with

$$\phi_{\alpha}^N(\vec{r}) = \sum_i U_{\alpha i} \phi_i(\vec{r}) \quad (13)$$

The eigenvalues λ_{α} are the occupation number of the orbitals: $\lambda_{\alpha} = 1$ for a fully occupied orbital, $\lambda_{\alpha} = 0$ for an empty one and $0 < \lambda_{\alpha} < 1$ for the interesting case of active orbitals responsible for electronic correlations. Fig. 8 shows these occupation numbers for different basis sets of increasing size. We see that, as expected, only a few orbitals are occupied more than 10^{-3} , but as we saw on Fig. 3, even lowly filled orbitals are necessary to obtain accurate energies. We also observe a convergence towards the continuum limit as the size of the basis set is increased.

Basis set error ϵ_{bs} for a few selected molecules

In this section we try and assess the potential gain in accuracy that could be reached using tensorized orbitals. It is an extension of the discussion around Fig. 3 of the main text.

Fig.9 shows the energy versus number of orbitals M for a CCSD(T) calculation of four molecules (H_2 , H_2O , N_2 and O_2). The triangles correspond to standard CCSD(T) calculations in the Gaussian basis set cc-pvXz with X =

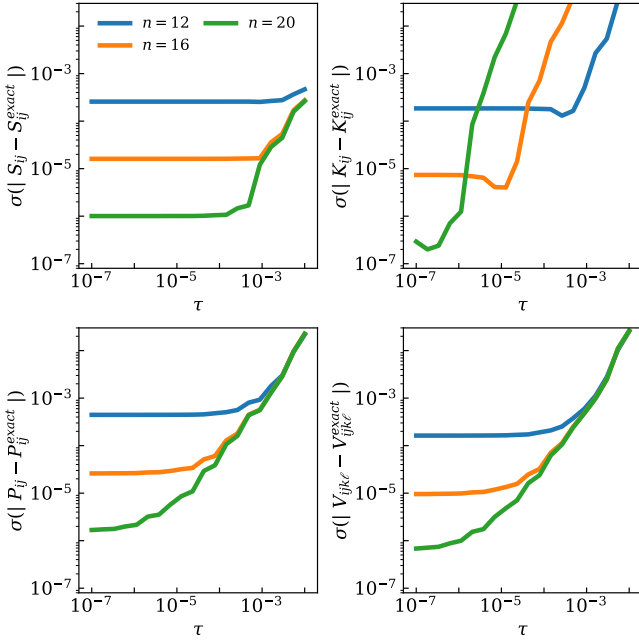


FIG. 7. Error on the matrix elements for varying tolerance τ . Here, the error is defined as the standard deviation of the distance between the target and the obtained result: $\sigma(|S_{ij} - S_{ij}^{\text{exact}}|)$. The matrix elements were computed for H_2 with the basis set cc-pvDz ($M = 10$).

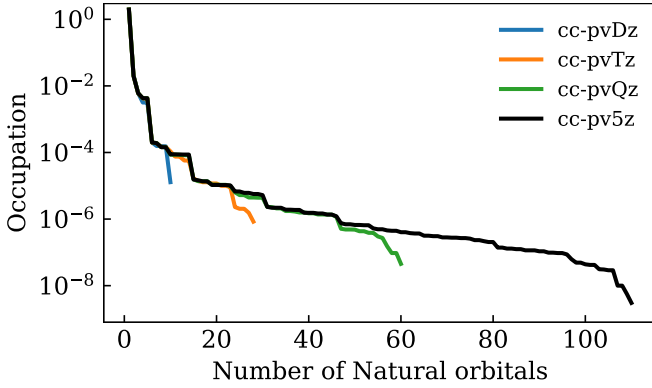


FIG. 8. Occupation levels of each eigenstate of the 1-body density matrix $\rho_{ij} = \langle c_i^\dagger c_j \rangle$. This is computed here for the H_2 molecule in different basis sets.

D (blue), T (orange), Q (green) and 5 (pink). The black circle corresponds to the continuum limit obtained using the algorithm described in the main text (essentially calculating the M most important natural orbitals from a cc-pvQz calculation and checking that the results are converged with respect to the basis sets, i.e. unchanged when doing the same procedure with the cc-pv5z basis set).

Two pieces of information can be extracted from this figure. First the last point of the continuum limit, which corresponds to a calculation with the same value of M as

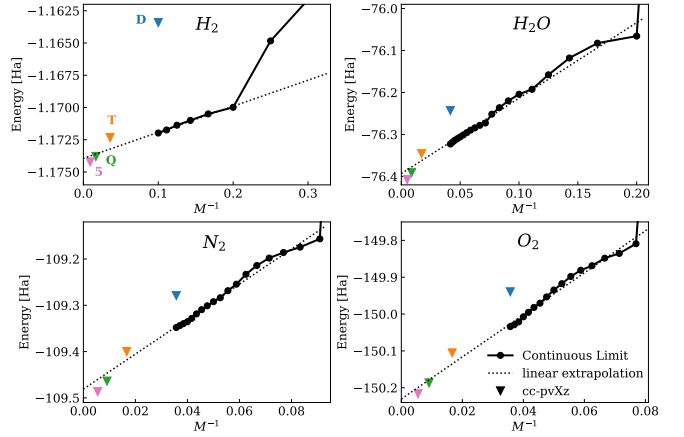


FIG. 9. Couple cluster CCSD(T) calculation of the energy versus number of orbitals M for a few molecules. Colored triangles: standard calculation using the cc-pvXz basis set with $X = D$ (blue), T (orange), Q (green) and 5 (pink). Black circles: optimum orbitals in the continuum limit (constructed from natural orbitals, see text). Dotted lines: linear extrapolation from a simple linear regression. Molecular parameters: $d_{H-H} = 1.40108a_0$; $d_{H-O} = 1.80869a_0$; $\theta_{H_2O} = 104.225^\circ$; $d_{N-N} = 2.07515a_0$ and $d_{O-O} = 2.270a_0$.

a cc-pvDz calculation is consistently more accurate than the bare cc-pvDz result by a large value of $100mHa$ or more (except for H_2). Second, the results in the continuum limit are intrinsic, i.e. they depend only on M not on how the basis set have been constructed. Hence the M -dependance of the energy which is crucial for the extrapolation to the $M \rightarrow \infty$ CBS limit has its origin in the actual form of the correlations in the molecule, not in the ability of the scientist to construct a basis set that "exptrapolates well". Hence we conjecture that working in the continuum limit - which should be possible with tensorized orbitals - will lead to significant improvement on the accuracy of the CBS extrapolation. To illustrate this point we have performed a linear extrapolation of our continuum limit (dotted line) using a simple linear regression. The results consistently provide an increase of precision of the order of a factor ten with respect to the cc-pvDz calculation (which corresponds to the largest value of M considered in the continuum limit). For our H_2 benchmark where the exact energy is known, the calculation in the cc-pvDZ basis set yields an error of 11.1 mH while the linear extrapolation to the CBS limit has an error of 0.6 mHa. Similarly for H_2O , the cc-pvDz error is 150 mHa while the linear extrapolation yields an error of 18 mHa.

Single orbitals: comparison between Gaussians and DMRG

In Table I we showed that constructing orbitals directly with DMRG for ions yields very accurate energies, sig-

nificantly better than what was obtained with Gaussians using very large basis set. Here, we examine the corresponding probability distributions and show that these small differences in energy are associated to significant differences. The results are shown in Fig. 10 for H_2^+ (left) and HeH^{2+} (right). The plot shows $|\phi(x, y, z)|^2$ versus x for a fixed value of y and $z = 0$ ($y = z = 0$ corresponds to the nuclei-nuclei axis). Full lines are converged DMRG result (essentially exact) and dashed line are obtained from a linear combination of Gaussians with the very accurate cc-pv5z basis set. For H_2^+ , we observe that the combination of Gaussian displays significant deviations, especially close to the nuclei and in the tails (here in between the two protons), as expected. The discrepancy is harder to observe for HeH^{2+} with the bare eye. However, the error on the energy (a global probe) is larger in this case. Note also that there is considerable knowledge and work hidden in the construction of the Gaussian basis set while the DMRG approach is fully agnostic and automatic.

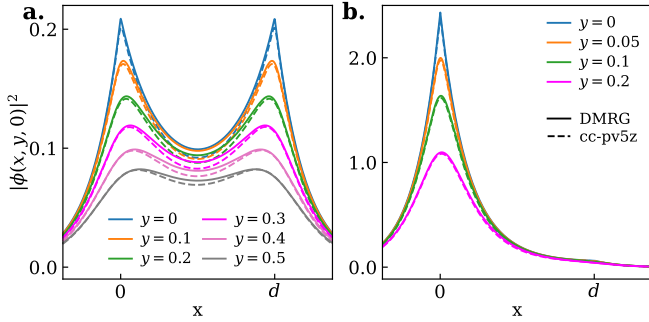


FIG. 10. Profiles of density of probability $|\phi(x, y, z = 0)|^2$ versus x (fixed y) for the ground state of H_2^+ (a.) and HeH^{2+} (b.). Solid line: DMRG result; dashed lines: best combination of Gaussian orbitals within the cc-pv5z basis set. $d_{H-H} = 2 a_0$ and $d_{He-H} = 1.4634 a_0$.

Role of the bits ordering in the MPS rank.

For the Quantics decomposition in 3D, several orderings of the bits are possible. We previously choose the *grouped ordering* in which the indices are grouped by the coordinate they encode :

$$\Phi_{x_1 \dots x_n y_1 \dots y_n z_1 \dots z_n} = \prod_{a=1}^n M_a(x_a) \prod_{a=1}^n M_{a+n}(y_a) \prod_{a=1}^n M_{a+2n}(z_a) \quad (14)$$

However, it is also possible to consider the *interleaved ordering* : the indices are gathered by similar scales. It amounts to substituting Eq. (7) with :

$$\Phi_{x_1 y_1 z_1 x_2 y_2 z_2 \dots x_n y_n z_n} = \prod_{a=1}^n M_{3a}(x_a) M_{3a+1}(y_a) M_{3a+2}(z_a) \quad (15)$$

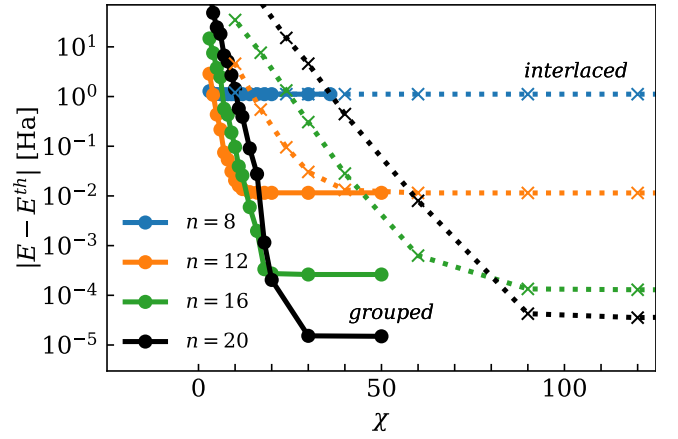


FIG. 11. Error on the total energy of the LiH molecule in the STO-6g basis set versus bond dimension χ of the orbitals. This is a benchmark to show the accuracies of the MPS computed integrals compared to the exact gaussian based. The resolution is done at the CCSD(T) level. Distance between the nuclei: $2.8571a_0$. All calculations with *grouped ordering* are done with compression tolerance $\tau = 10^{-10}$ and for *interleaved ordering* with $\tau = 10^{-5}$. The reference calculation uses the pyscf package [25].

The choice of the encoding has an important impact on the bond dimensions of the MPS. For example, Gaussians are interpolated within numerical accuracy with $\chi = 11$ with *grouped ordering* but for *interleaved*, the same accuracy requires going above $\chi = 150$. The laplacian MPO has $\chi = 4$ in 3D with *grouped ordering* but $\chi = 7$ with *interleaved ordering*. Overall, it seems that for the present application, *grouped ordering* is significantly better. This is shown in Fig. 11 which reproduces the results of Fig.2 for both orderings.

Multi-orbital MPS.

The different orbitals used in the calculations of this article are actually often very similar and only rotated, translated or dilated. For this reason, it would be efficient to combine all the orbitals in a single MPS. Such an MPS only requires an additional outer-leg to account for the different indices of the orbital. Therefore, we briefly consider the following encoding of all orbitals in a single MPS:

$$\Phi_{\alpha\vec{r}} = M_0(\alpha) \prod_{a=1}^n M_a(x_a) \prod_{a=1}^n M_{a+n}(y_a) \prod_{a=1}^n M_{a+2n}(z_a) \quad (16)$$

The computations of the matrix elements for such an MPS are greatly simplified: a single MPS.MPO.MPS contraction would yields the entire matrices S_{ij} , H_{ij} and similarly for the $\Phi_{\vec{r}}^{ij}$ and V_{ijkl} respectively. We leave such a program for future work and limit ourselves to investigating the impact on the rank χ of this scheme.

The results of a few numerical experiments are displayed in Fig. 12. We observe that overall the bond dimension at given accuracy increases linearly with the number of orbitals $\chi \propto M$. We also observe that the more the basis sets are redundant (e.g. correspond to simple translations/rotations of a few primitives), the smaller the slope. The storage of the orbitals using single-orbital tensorised orbitals scales as M against M^2 for the present scheme. Multi-orbital MPS therefore do not seem to be advantageous memory wise. However the calculation of the Coulomb matrix elements scales as M^4 for both single and multiple orbitals MPS, possibly with a significantly smaller prefactor for the latter. It follows that such a scheme could be advantageous when this computation becomes significant.

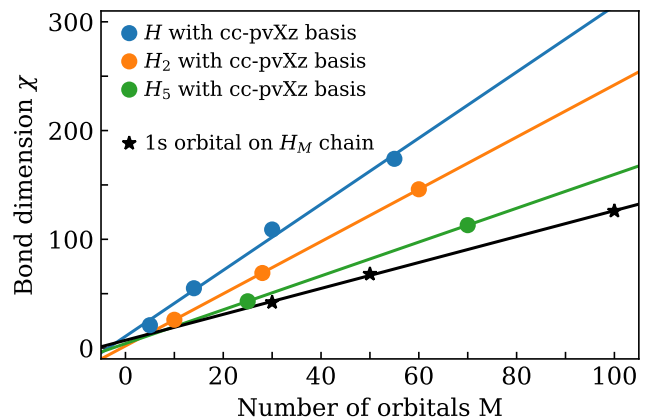


FIG. 12. Bond dimension of a single multi-orbital MPS for an accuracy of $\epsilon_{OS} = 10^{-4}$ versus the total number of orbitals M used to describe the molecular chain. We chose the standard cc-pvXz basis sets for chains of hydrogen (H , H_2 and H_5 , circles). From left to right $X = D, T, Q, 5$. We also considered the case of a single Slater orbital (1s) for an increasingly large chain H_M (stars). The symbols correspond to the data, the lines to linear interpolations. All calculations are done with $n = 12$ and the step between atoms is $d = 1.4a_0$. For chains longer than 20 atoms, we started a new line of atoms.